Computational Materials Science 45 (2009) 774–782

Contents lists available at ScienceDirect

Computational Materials Science

journal homepage: www.elsevier.com/locate/commatsci

Finite element crystal plasticity analysis of spherical indentation in bulk single crystals and coatings

O. Casals *, S. Forest

Centre des Matériaux, Mines ParisTech, CNRS UMR 7633, 91003 Evry Cedex, France

ARTICLE INFO

Article history:
Received 30 August 2008
Received in revised form 30 September 2008
Accepted 30 September 2008
Available online 26 November 2008

Keywords:
Micro-indentation
Crystal plasticity
Contact anisotropy
Coatings and thin films

ABSTRACT

The purpose of the present work is to investigate the anisotropy in the contact response of f.c.c and h.c.p single crystals. To this aim, spherical indentation experiments were simulated at a meso-scale, which is relevant to the interpretation of instrumented indentation experiments and micro-hardness tests in bulk single crystals and coatings. Within this framework, both the instrumented indentation load (P)-penetration depth (h_s) curves and the pile up or sinking-in patterns developed around the indentation imprint were analyzed. The detailed assessment of plastic zone morphology and plastic strain localization features was also addressed to complete the micro-mechanical analysis of indentation experiments. An important outcome from the present work is the identification of very specific and orientation dependent locations within the film–substrate interface, where plastic strain localizes as indentation proceeds. These findings can be significant on the prediction of delamination and potential failure of coatings and thin films.

1. Introduction

Mechanical property characterizations of small components and thin films are routinely performed using indentation techniques. Under the local contact solicitations developed during indentation experiments, only few micro-constituents, or even individual grains, actually rule the mechanical response of the component. Within this context, the classical macroscopic interpretation of indentation data may hardly apply due to the intrinsic anisotropy in both the elastic and plastic responses of single crystals. Hence, the use of continuum isotropic models and simplified power-law strain hardening relations, which are conventionally used for the analysis of indentation in polycrystalline metals [1–3] becomes at least debatable [4]. Alternatively, spherical indentation simulations can be performed within the framework of classical crystal plasticity models [5,6]. These constitutive models allow for the analysis of the intrinsic influence of the anisotropic plastic flow of different crystalline metals (i.e. f.c.c. copper and h.c.p. zinc single crystals) upon the contact response. It must be noted that the length scale under consideration is still large enough as to neglect any size effect associated to the nucleation and interaction of a reduced number of dislocations and to the activation of dislocation multiplication sources beneath the indenter. Hence, dislocation and molecular dynamics simulations, which are suitable for the numerical analysis of the contact yield point phenomenon [7] and ultra-low load nanoindentation experiments [8], remain out of the scope of the present research.

2. Computational method

2.1. Constitutive equations

In the present simulations, a fully anisotropic elasticity tensor was considered for modelling the elastic response of all single crystals (see Table 1). Furthermore, the crystal plasticity model initially proposed in [9] was used for the simulation of the corresponding plastic behavior. A large deformation formulation, accounting for finite strains and rotations, is adopted through the entire work since relatively large plastic strains are readily attained close to the contact zone. The kinematics of the model conform to the classical multiplicative decomposition of the deformation gradient

$$\mathbf{F} = \mathbf{F}^{\mathbf{e}}\mathbf{F}^{\mathbf{p}}, \tag{1}$$

whose plastic part, $\mathbf{F}^{\mathrm{p}}$, is assumed to be solely related to slip deformation occurring in discrete crystallographic slip systems characterized by unit vectors lying along the slip direction, $\mathbf{m}^{\mathbf{s}}$, and the normal to the slip plane, $\mathbf{n}^{\mathbf{s}}$.

$$\dot{\mathbf{F}}^{\mathrm{p}}\mathbf{F}^{\mathrm{p}\,-1} = \sum_{s=1}^{n} \dot{\gamma}^{s}\mathbf{m}^{\mathbf{s}} \otimes \mathbf{n}^{\mathbf{s}} \tag{2}$$

* Corresponding author.
E-mail addresses: ovidi.casals@ensmp.fr, ovidi.casals@compassis.com (O. Casals).

0927-0256/$ - see front matter © 2008 Elsevier B.V. All rights reserved.
doi:10.1016/j.commatsci.2008.09.030

Table 1
Anisotropic elastic properties of copper and zinc single crystals. All reported values are in MPa.

Copper (f.c.c)		Zinc (h.c.p.)			
C_{11}	159,300	C_{11}	165,000	C_{44}	33,475
C_{12}	122,000	C_{22}	165,000	C_{55}	19,800
C_{44}	81,000	C_{33}	61,800	C_{66}	19,800
				C_{12}	31,100
				C_{23}	50,000
				C_{31}	50,000

A rate dependent flow rule is adopted to facilitate the determination of a unique set of active slip systems [10]

$$\dot{\gamma}^s = \left\langle \frac{|\tau^s| - r^s}{K} \right\rangle^n \operatorname{sign}(\tau^s), \tag{3}$$

where τ^s is the resolved shear stress, r^s is the corresponding isotropic strain hardening variable, and K and n are viscosity parameters. A non-linear hardening rule, that governs the evolution of the hardening variable, completes the crystal plasticity constitutive model

$$r^s = r_o + q \sum_{r=1}^{n} h^{sr}(1 - \exp(-bv^r)), \tag{4}$$

In Eq. (4), r_o is the critical resolved shear stress, h^{sr} is a hardening matrix accounting for self ($r = s$) and latent ($r \neq s$) hardening, v^r is the cumulated plastic slip for system (r) and $\dot{v}^r = |\dot{\gamma}^r|$. Finally, q and b are phenomenological constants. Parameters for copper and zinc single crystals were taken from the literature [11–13] were different sets are proposed for best fitting experimental data obtained under different conditions (i.e. uniaxial tensile tests, cyclic loading, etc.). In the present work, the final set of parameters was chosen as to match, within reasonable accuracy, the anisotropic uniaxial behavior of the crystals while reproducing sensible hardness values during the simulation of indentation experiments. The anisotropic hardening behavior of Cu is enhanced by the heterogeneous hardening matrix h^{rs} taken for the $\{1\,1\,1\}\langle 0\,1\,1\rangle$ family of slip systems. Specifically, h_1 in Table 2 accounts for self-hardening (i.e. $s = r$) while $h_2 - h_6$ refer to the remaining independent components of latent-hardening. In this sense, in f.c.c crystals there only exist five distinct slip system interactions, leading to at most five independent components of the matrix. By contrast, anisotropy on Zn single crystals is mainly accounted for by the variety of plastic parameters adopted for different slip system families. In this case, the hardening matrix is assumed completely isotropic so that both self (h_1) and latent-hardening (h_2) are taken equal to unit in all slip system families. No additional interaction between different slip system families is considered.

In those simulations concerning indentation of thin films on hard substrates, a fully isotropic elastic response was assumed for modeling the substrate. Although this implies an important simplification on the actual behavior of the material, it is a suitable first approximation to the problem. A silicon substrate ($E = 150$ GPa) was considered for copper thin films, while a steel substrate ($E = 210$ GPa) was chosen in the case of zinc crystal thin films. These material combinations were taken for being representative of true systems that can be found in electronics and surface technology applications, respectively. In both cases the substrate is much harder than the coating, so it is expected that for even relatively large indentations the substrate may remain within its elastic regime.

Table 2
Crystal plasticity parameters for the distinct slip system families of copper and zinc single crystals.

	Cu (oct)	Zn (bas)	Zn (pyr)	Zn (pris)
K (MPa)	5.0	1.0	10.0	10.0
n	10.0	5.0	5.0	5.0
$r_\circ$ (MPa)	35.0	1.5	15.0	22.5
q (MPa)	6.0	1.0	15.0	22.0
b	15.0	3.0	30.0	10.0
h_1	1.0	1.0	1.0	1.0
h_2	4.4	1.0	1.0	1.0
h_3, h_4, h_5	4.75			
h_6	5.0			

2.2. Finite element simulations

All simulations were performed with the finite element code Zebulon. 3D meshes were constructed following the same mesh refinement strategy as in [3]. This mesh design has been proved to provide extremely accurate solutions for several axisymmetric [14,15] and 3D [16] contact problems dealing with both, sharp and spherical indentation experiments. A typical finite element model in the present simulations contains about 21200 eight-node linear brick elements (c3d8), and consists of various zones of different element density, connected through a structured transition region optimized to minimize the distortion of field variables within the plastic zone (see Fig. 1). The simulations are conducted under displacement control so that maximum penetration depth is kept constant in all cases ($h_s^{max} = 3.5$ μm). This ensures that the maximum contact radius remains always smaller than $L/50$, being L the radial dimension of the cylindrical sample. This condition minimizes the specimen's boundary effect and allows for the recovery of the Boussinesq's solution far away from the contact area [16].

Only well defined crystallographic planes were indented in order to take advantage from the partial symmetry of the resulting contact configurations. Following this modeling strategy, only reduced portions of the crystal sample actually need to be explicitly modeled by applying pertinent boundary conditions at the corresponding symmetry planes. From this procedure, complete information of the full 3D deformation patterns can be actually obtained at a lower computational cost. One of the finite element

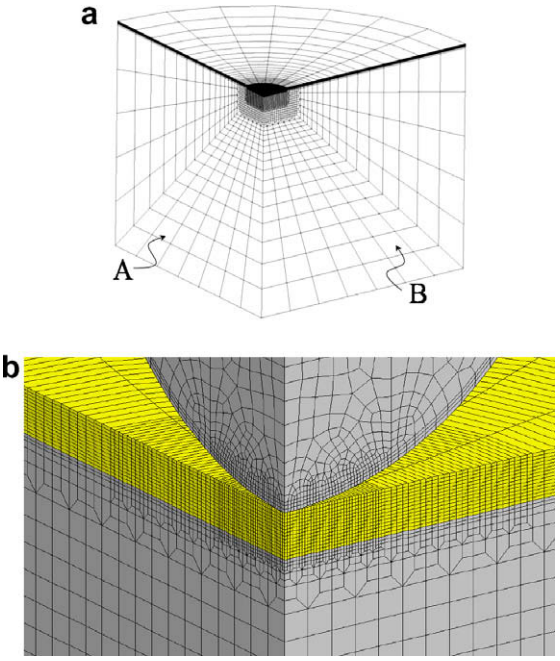

Fig. 1. Cross sectional view of one of the models used in the simulations. A detail of the mesh close to the contact zone is shown in (b) where the coating region appears in yellow. (For interpretation of the references to colour in this figure legend, the reader is referred to the web version of this article.)